


**RESEARCH ARTICLE**

WILEY

# Dynamic domain kinematic modelling for predicting interflow over leaky impeding layers

Menberu Meles Bitew<sup>1,2</sup>  | C. Rhett Jackson<sup>2</sup> | David C. Goodrich<sup>1</sup> | Seth E. Younger<sup>2</sup> | Natalie A. Griffiths<sup>3</sup> | Kellie B. Vaché<sup>4</sup> | Benjamin Rau<sup>5</sup>

<sup>1</sup>USDA ARS, Southwest Watershed Research Center, Tucson, Arizona

<sup>2</sup>Warnell School of Forestry and Natural Resources, University of Georgia, Athens, Georgia

<sup>3</sup>Climate Change Science Institute and Environmental Sciences Division, Oak Ridge National Laboratory, Oak Ridge, Tennessee

<sup>4</sup>Department of Biological and Ecological Engineering, Oregon State University, Corvallis, Oregon

<sup>5</sup>USDA Forest Service, Savannah River Forestry Sciences Lab, Aiken, South Carolina

**Correspondence**

Menberu Meles Bitew, USDA ARS, Southwest Watershed Research Center, 2000 E Allen Road, Tucson, AZ 85719.  
Email: menberu.bitew@ars.usda.gov

**Funding information**

Department of Energy-Savannah River Operations Office through the U.S. Forest Service, Grant/Award Number: DE-AI09-00SR22188; U.S. Department of Energy's Bioenergy Technologies Program, Grant/Award Number: DE-AC05-00OR22725

**Abstract**

Traditional Boussinesq or kinematic simulations of interflow (i.e., lateral subsurface flow) assume no leakage through the impeding layer and require a no-flow boundary condition at the ridge top. However, recent analyses of many interflow-producing landscapes indicate that leaky impeding layers are common, that most interflow percolates well before reaching the toe slope, and therefore, the downslope contributing length is shorter than the hillslope length. In watersheds characterised by perched interflow over a low conductivity layer through permeable topsoil, interflow with percolation may be modelled with a kinematic wave model using a mobile upslope boundary condition defining the hillslope portion contributing interflow to valleys. Here, we developed and applied a dynamic interflow model to simulate interflow using a downslope travel distance concept such that only the active contributing length is modelled at any time. The model defines a variable active area based on the depth of the perched layer, the topographic slope and the ratio of the hydraulic conductivity of topsoil to that of the impeding layer. It incorporates a two-layer soil moisture accounting water balance analysis, a pedo-transfer function, and percolation and evaporation routines to predict interflow rates in continuous and event-based scenarios. We tested the modelling concept on two sets of data (2-year dataset of rainfall observations for the continuous simulation and a multi-day irrigation experiment for the event simulation) from a 121-m-long open interflow collection trench on an experimental hillslope at the Savannah River Site, South Carolina. The continuous model simulation partially represented the observed interflow hydrograph and perched water depth in the experimental hillslope with correlation coefficients of 0.85 and 0.35, respectively. Model performance improved significantly at event-scale analysis. The modelling approach realistically represents interflow dynamics in hillslopes with leaky impeding layers and can be integrated into catchment-scale hydrology models for more detailed hillslope process modelling.

**KEYWORDS**

Boussinesq, downslope travel distance, hillslope, interflow modelling, kinematic, leaky impeding layer, open trench

## 1 | INTRODUCTION

Properties of surface soil layers and shallow impeding layers play an important role in partitioning rainfall to infiltration, percolation, evapotranspiration (ET) and streamflow generation. These soil properties particularly affect interflow dynamics. Interflow is the portion of infiltrated precipitation that travels downslope over an impeding layer towards a stream or river valley where it may feed saturated areas, the riparian aquifer or the stream itself. Interflow, or shallow lateral flow or slope-parallel flow in hillslopes (Asmussen & Ritchie, 1969; Dunne, 1978; Minshall & Jamison, 1965), was initially explained by anisotropic control (e.g., Zaslavsky & Sinai, 1981). Later, interflow was conceptualised as an important flow component on steeper hillslopes with high conductivity surface soils and an impeding layer that is an impermeable or semi-permeable soil layer at shallow depth (e.g., Flügel & Smith, 1998; Sloan & Moore, 1984; Tromp-van Meerveld, Peters, & McDonnell, 2007). Such flow situations potentially occur over a variety of impeding layers including argillic horizons, fragipans, glacial tills and bedrock (Bishop, Seibert, Kohler, & Laudon, 2004; Buttle & McDonald, 2002; Du et al., 2016; McGlynn, McDonnell, Shanley, & Kendall, 1999; Newman, Campbell, & Wilcox, 1998; Tromp-van Meerveld & McDonnell, 2006; Wilcox, Newman, Brandes, Davenport, & Reid, 1997).

Many studies have observed the simultaneous occurrence of lateral flow and percolation or leakage through pedogenic and lithologic impeding layers. Newman et al., (1998) and Wilcox et al., (1997) reported leakage and also significant lateral subsurface flow over a series of clay-rich restrictive layers for a semiarid ponderosa hillslope experiment. Graham, van Verseveld, Barnard, and McDonnell (2010) and Graham and McDonnell (2010) showed that bedrock topography and permeability strongly control the partitioning of the water balance in a hillslope in the Maimai catchment. When percolation or leakage through the impeding layer is considered, most perched water from the upper reaches of the hillslope percolates through the impeding layer before reaching the valley, effectively reducing the interflow contributing area to the lower slopes (Du et al., 2016; Jackson et al., 2016; Jackson, Bitew, & Du, 2014; Klaus & Jackson, 2018). The contributing distance increases as infiltration from precipitation increases, creating a dynamic interflow contributing area. Leakage through impeding layers and dynamic contributing zones can be captured by two and three-dimensional models using Richards equation (e.g., Broda, Larocque, & Paniconi, 2014; Broda, Paniconi, & Larocque, 2008; Broda, Paniconi, & Larocque, 2011; Zaslavsky & Sinai, 1981). For many modelling applications, however, simpler algorithms, using either Boussinesq or kinematic assumptions, are desired for modelling interflow contributions to valleys and streams. However, few of these simpler models have incorporated leakage through impeding layers for modelling lateral flow. Beven (1981) formulated a lateral outflow model on hillslopes with infiltration using a linearization of the Boussinesq equation. Other similar kinematic wave and empirical approximation procedures using the Duijuit-Forchheimer equation were also implemented to compute interflow from storage balance over planar surfaces (e.g., Koussis, Smith, Akylas, &

Tombrou, 1998; Pi & Hjelmfeld, 1994; Schroeder, Gibson, & Smolen, 1983). A wide range of kinematic approximation-based modelling approaches for assessing lateral flow and near-surface aquifer dynamics have been developed over the years (e.g., Beven, 1981; Jackson & Cundy, 1992; Koussis et al., 1998; Pi & Hjelmfeld, 1994; Schroeder et al., 1983; Sloan, Morre, Coltharp, & Eigel, 1983; Smith & Hebbert, 1983; Troch, van Loon, & Hilberts, 2004). All of these models require a no-flow boundary condition at the ridgetop and most have neglected leakage through the impeding layer (e.g., Jackson & Cundy, 1992; Troch, Paniconi, & van Loon, 2003).

Observations in an experimental hillslope at the Savannah River Site, South Carolina, demonstrated that the effective downslope travel distance is time-variant, expanding during rainfall and contracting afterward (Du et al., 2016; Jackson et al., 2016). Here, we developed and evaluated a dynamic domain interflow model that only simulates the interflow contributing area and does not require a ridgetop no-flow boundary. The model quantifies the active hillslope area that delivers interflow to the stream or adjacent water body using a downslope travel distance that is a combination of the Darcian and kinematic downslope flow equations. Flow through the unsaturated layers was described using the water balance formulation to compute changes in storage over a discrete time step. The central objective of this model formulation is to estimate the downslope travel distance and quantify the portion of the rainfall that leaves the hillslope as interflow. We used hydrometric time series and soil layer information together with measurements of the perched water level above the impeding layer and trench flow from an open trench in an experimental hillslope in the Upper Coastal Plain of South Carolina, USA, to formulate, test and validate the model. The model requires soil horizon parameters including hydraulic conductivity, porosity, thickness, depth, water content at field capacity, wilting point and saturation. The modelling approach is novel in that it simulates only the active areas and quantifies both near-surface interflow as perched saturated flow and percolation through the impeding layer as an unsaturated flow.

## 2 | DOWNSLOPE TRAVEL DISTANCE MODELLING CONCEPT

Jackson et al., (2014) developed a model that predicts how far water can travel down a hillslope above an impeding layer before it percolates. In this approach, flow above the impeding layer is viewed as having a normal (perpendicular) flow component controlled by leakage through the impeding layer and a downslope (slope-parallel) component controlled by slope and topsoil conductivity. The resultant flow path is thus not slope-parallel but includes a downward normal component such that water moves a certain distance downslope before percolating (see flow path in Figure 1). We used this concept to develop a dynamic interflow prediction tool for continuous and event-based scenarios. This work expands on the formulation of the downslope travel distance (Equation 1) by Jackson et al., (2014) for precipitation events and flow in hillslopes with a leaky lens at shallow

depth (Figure 1), by incorporating flow systems across the entire hillslope and building a more complete representation of hydrological processes for predicting interflow. The flow processes include vertical unsaturated flow through the topsoil, combined lateral flow down the slope and normal flow at the interface with the impeding layer, normal saturated flow through the impeding layer and vertical unsaturated flow below the bottom of the impeding layer. The downslope travel distance ( $L_D$ ) equation in Jackson et al., (2014) was formulated by adding two orthogonal Darcy velocities,  $q_x$  and  $q_n$  (Figure 1), and using the resultant to determine the downslope distance a water parcel travels before traversing the saturated depth above the impeding layer.

$$L_D = (K_u/K_L) (\sin\alpha/(N + C_n)/C_n) N \quad (1)$$

where  $\alpha$  is the slope of the hillslope,  $C_n$  is the thickness of the impeding layer, and  $N$  is the normal thickness of the perched water table.  $K_u$  and  $K_L$  are the hydraulic conductivities of the topsoil and the impeding layer, respectively.

We assume that once water enters the impeding layer, the flow direction becomes vertical and percolates to groundwater. We computed the portion of perched water that could leave the system as interflow using the analysis of travel distance from the point of infiltration and its flow path towards the stream. Considering interflow as the portion of the infiltrated water that enters the stream channel (always above the main groundwater level), water will appear as interflow only if  $L_D$  is longer than the distance to the variable saturation edge. The variable saturation region is the riparian region in the watershed where interflow and groundwater meet, possibly resulting in overland flow in the riparian region. The interflow condition is true if  $L_D \geq Nr_D - V_d$ , where  $Nr_D$  is the possible flow path distance down the

hillslope.  $V_d$  is the variable saturation distance, which is mainly dependent on the groundwater level and the stream valley landscape (e.g., this value is zero where groundwater is below the riparian soil surface).  $V_d$  expands and contracts based on the extent of groundwater in contact with the surface. The portion of the hillslope where perching develops and also contributes interflow to the stream is referred to as the active area. This definition of the active area combines the variable active and contributing areas indicated in Ambrose (2004). Areas that do not produce interflow are inactive. The active area of interflow delivery features a mobile upslope boundary condition defined by the magnitude of the downslope travel distance and the position of the interflow receiving water body in the landscape. The travel distance depends on the depth of perching and the ratio of the downslope flow component to the normal flow component. To examine the relationship between the effective precipitation depth that results in perching, the active area and downslope travel distances, we used a range of precipitation depth scenarios of 0–1,300 mm in soil with a porosity of 0.35.

## 2.1 | Model structure

We present two versions of the dynamic interflow model: a continuous model and an event-based model, implemented as a two-layer soil water balance. The continuous model incorporates time-variant processes such as evapotranspiration (ET), infiltration and percolation and computes the interflow rate at hourly time steps based on the available moisture gradients and evaporative energy. The event-based formulation targets specific events within a short window of time, recognizing that only those events where rainfall depth in excess of the deficit in the topsoil layer results in perching.

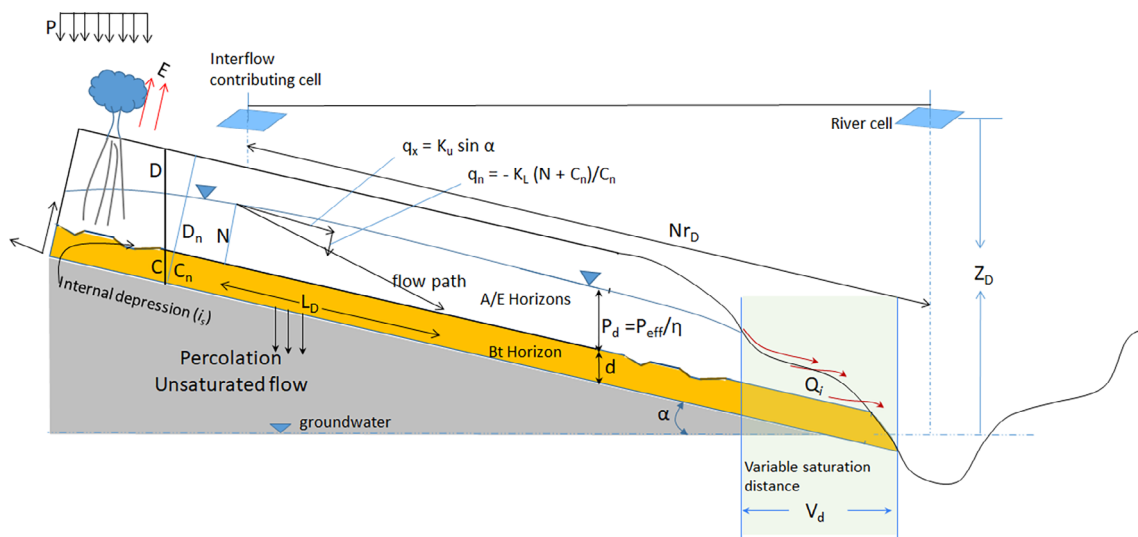


**FIGURE 1** Schematic of hillslope and interflow generation processes in perched Boussinesq (slope-parallel) flow with percolation through a leaky impeding layer (argillic/Bt horizon) underlying a highly conductive topsoil layer (A/E horizons). This figure was adapted from Jackson et al., (2014) and modified to derive flow equations for interflow prediction using the downslope travel distance concept. See the table at the beginning of the paper for parameter definitions

### 2.1.1 | Continuous interflow model

The continuous modelling framework (Figure 2a) includes soil water, storage and abstraction dynamics. It establishes the moisture content of the soil layers at any time  $t$ , based on the amount of transpiration, rainfall and percolation through the impeding layer. The data inputs into the continuous model include hourly precipitation, potential ET and the depths/thicknesses and properties of the two soil layers (in this study, it is based on the characteristics of the experimental hillslope at the Savannah River Site). We divided the soil into two layers for water balance calculations. The first layer is the unsaturated portion of the top sandy soil above the perched water table and the second layer consists of the saturated portion of the top sandy soil and the entirety of the impeding layer. The impeding layer (argillic Bt horizon) is assumed to have the same slope as the surface, but in reality, the subsurface layer is undulating. In the absence of excess rainfall that creates perching, the thickness of Layer 1 is at its maximum, which is equal to the thickness of the top sandy soil. Layer 2 is the saturated portion of the two layers, which includes the perched water depth of the sandy soil and the underlying impeding (clay) layer through which percolation occurs. In the model, soil water content greater than field capacity in the top layer is assumed to be stored above the impeding layer, decreasing the thickness of Layer 1 depending on the amount of perching ( $P_d$ ) in the hillslope. When there is no perching in the hillslope, the thickness of Layer 2 will be at its minimum, which is the thickness of the impeding layer ( $d$ ). The limitation of this assumption is that the maximum soil moisture of Layer 1 is always field capacity unless an exceptional excess rain fills up the entire column to the top. This assumption ignores the possibility of preferential flow that results in more rapid movement of water than matrix flow.

Perching and/or interflow begins after storage deficits are filled in the hillslope system. The deficits include the amount of precipitation intercepted by the canopy, the rainfall necessary to bring both the topsoil and the impeding layer past field capacity (soil moisture deficit), the additional water required to saturate the impeding layer and the water necessary to fill the depressions in the impeding layer surface (see Equation 2). The amount of rainfall minus the hillslope losses is termed effective precipitation ( $P_{eff}$ ) throughout this paper.  $P_{eff}$  is the portion of precipitation that is responsible for perched water above the impeding layer and ultimately flows over the impeding layer. The perching depth ( $P_d$ ) over the impeding layer (Equation 3) is given as a function of the porosity of the topsoil layer ( $\eta$ ) and the effective precipitation.

$$P_{eff} = P - C_{in} - (\theta_{fc} - \theta_i)(T - P_d - i_s - (\theta_{afc} - \theta_{ai})d) \quad (2)$$

$$P_d = P_{eff} / \eta \quad (3)$$

where  $P$  is the precipitation at a time  $t$ ,  $C_{in}$  is the canopy interception,  $\theta$  is the soil moisture content where 'fc' represents the field capacity, the subscript 'i' is the time in question and 'a' is the impeding layer identifier.  $T$  is the depth of the soil layer,  $P_d$  is the perched water depth,  $d$  is the thickness of the impeding layer and  $i_s$  is the detention storage volume over the surface of the impeding layer.

The evaporation routine includes the computation of actual evapotranspiration (AET) in the following order: canopy interception, the top sandy layer, the perched water table, the water stored in the internal depressions, and moisture held in the impeding layer until evaporative demand is satisfied or available water is exhausted. Canopy interception, a fraction of the total precipitation, is calculated as a

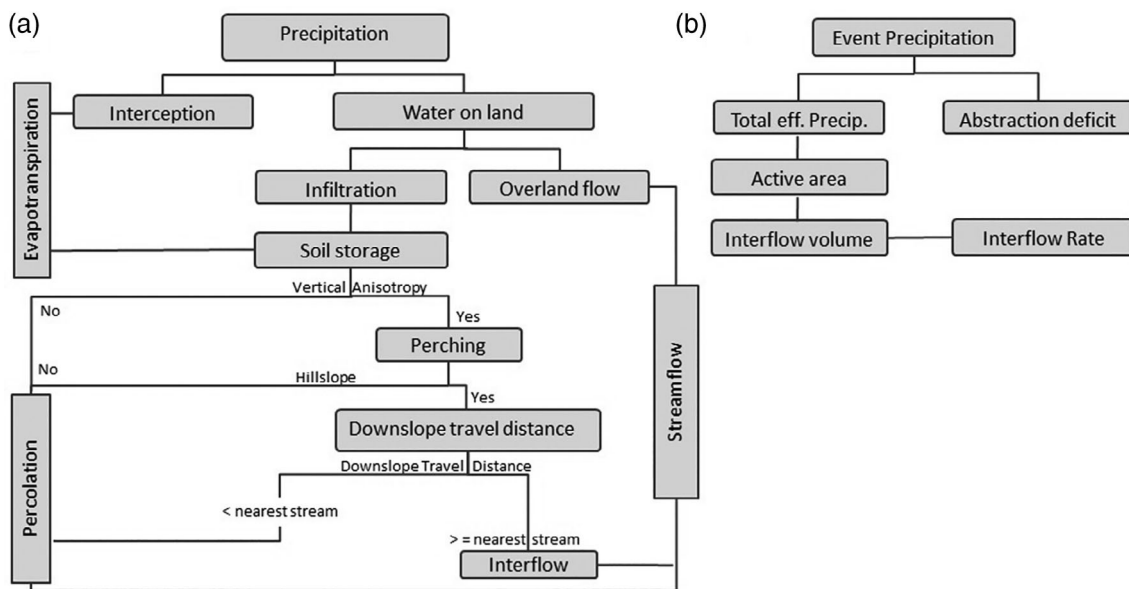


**FIGURE 2** Framework of the dynamic downslope travel distance model for interflow prediction. (a) Continuous modelling structure that dynamically updates hillslope processes at hourly time steps based on a two-layered soil water balance scheme, and (b) event-based interflow prediction model structure

function of LAI (leaf area index) and the canopy interception coefficient with the maximum interception amount not exceeding 2–3 mm during any given rainfall event (Kristensen & Jensen, 1975). The value of the maximum interception is determined by calibration. Hillslope losses also include water that evaporates during a period of perching from the top layer and the amount that percolates through the bottom of the impeding layer depending on the moisture deficit and the evaporative demand to be satisfied. The soil water balance calculation for both layers takes into account the evaporation and percolation amounts using sets of parallel 1-D explicit solution schemes. Soil moisture for subsequent hours is updated based on the two-layer water balance model (Equations 4 and 5) described below. The soil moisture in Layer 2 is updated based on the saturation/perching condition above the impeding layer. When perching is present, most of the evaporative demand draws water from the sandy layer, but in the absence of perching, the water for evaporative demand is extracted from the underlying impeding layer. For flow through the soil layers, a standard pedo-transfer function is applied to generate hydraulic conductivity values of the layers based on the updated soil moisture content (van Guchten, 1980). The use of a constant time step (1-hour) helped to represent the model assumptions realistically and reduce numerical errors (e.g., Clark & Kavetski, 2010). The two-layer water balance model is as follows:

$$\theta_{i+1} = \begin{cases} \theta_i + P_i - C_{in} - AET_s & \text{for } P_i - C_{in} < \theta_{fc} - \theta_i - AET_s \\ \theta_{fc} & \text{for } P_i - C_{in} \geq \theta_{fc} - \theta_i - AET_s \\ \theta_w & \text{for } \theta_i + P_i - C_{in} - AET_s \leq \theta_w \end{cases} \quad (4)$$

$$\theta_{ai+1} = \begin{cases} \theta_{asat} & \text{for } P_i - C_{in} < \theta_{asat} - \theta_i - AETas \\ \theta_{ai} + P_i - C_{in} - AETs - is - Kssin\alpha & \text{for } P_i - C_{in} \geq \theta_{afc} - \theta_{ai} - AETas \\ \theta_w & \text{for } \theta_{ai} + P_i - C_{in} - AETas \leq \theta_{aw} \end{cases} \quad (5)$$

where  $\theta_i$ ,  $\theta_{fc}$  and  $\theta_{sat}$  are the soil moisture contents at time  $t$ , at field capacity and at saturation, respectively.  $C_i$  is the canopy interception at any given time and AETs and AETas are the actual evapotranspiration values from Layers 1 and 2, respectively.

By combining the updated soil moisture content and the amount subsequently infiltrating through the impeding layer using downslope flow velocity (Boussinesq slope-parallel flow equation), the interflow rate ( $Q_i$ ) into a given stream is shown in Equation 6.

$$Q_i = \frac{K_u \sin\alpha L P_{effi}}{\eta_d} \quad (6)$$

where  $K_u$  is the hydraulic conductivity of Layer 1 for a given moisture content at a given time ( $i$ ),  $\alpha$  is the downslope surface angle from the horizontal and  $L$  is the length of stream receiving subsurface flow. When streams are fed with hillslopes from both sides of the river banks,  $L$  will be doubled in Equation 6.  $P_{eff}$  is the effective precipitation and  $\eta_d$  is the drainable porosity of the topsoil layer. The drainable porosity is the total porosity minus the soil moisture content at field

capacity.  $P_{eff}$  is updated for every time step ( $i$ ) as water leaves the perched system as interflow, evaporation or percolation to groundwater. The depth of perched water table will then continue to diminish over time.

## 2.1.2 | Event-based interflow model

In the case of the event-based analysis (Figure 2b), a similar water balance formulation in Equation 2 was used to compute the effective precipitation. The difference is that total hillslope losses/abstraction were calculated over the entire flow period in the continuous model instead of every hour in the event-based model, that is, all of the hillslope losses/abstraction deficiencies are subtracted from event rain to estimate the effective precipitation. Event rain, in this study, is defined as accumulated rainfall depth when the rainfall period is separated from the preceding and succeeding rain by 24 hr or more. After  $P_{eff}$  for the event rain was calculated, the total interflow volume ( $V_{Tint}$ ) was computed as a function of the effective precipitation, the amount of water leaking through the impeding layer and the active area (Equation 7). The total hillslope losses are the sum of interception, the total soil layer deficit (which brings the soil layer moisture content to field capacity), internal detention storage and estimated total ET over the perching period/interflow time ( $t_{int}$ ). The total soil moisture deficit for both layers was usually estimated based on the antecedent condition (rainfall prior to the event). The total evaporation was estimated by multiplying the interflow duration by the average hourly ET values for the site. Total interflow volume was calculated as:

$$V_{Tint} = A_a (P_{eff} - K_L \bar{t} (N + C_n) / C_n) \quad (7)$$

where  $V_{Tint}$  is the total interflow volume,  $A_a$  is the active area (i.e., the area of the interflow contributing hillslope) and  $\bar{t}$  is the average downslope travel time given as half of the sum of the interflow initiation time ( $t_o$ ) and the maximum interflow time ( $t_{int}$ ).  $K_L \bar{t} (N + C_n) / C_n$  represents the portion of water leaving the system via percolation. The missing variable in this formulation is the time component. We formulated the time component based on the distance water travels to reach the stream as interflow and the associated factors affecting the initiation of interflow for a given rainfall event. Equation 8 estimates the maximum interflow time ( $t_{int}$ ) as a function of the downslope travel time from the furthest upslope location of the active area and the period of overland flow in the variable saturation region with some estimates for interflow initiation time.

$$t_{int} = t_o + \frac{Nr_{Dmax}}{K_u \sin\alpha} + \frac{V_d^{1/3} n P_{eff}}{S^{0.5}} \quad (8)$$

where  $Nr_{Dmax}$  is the maximum interflow travel distance along the Euclidean distance to the stream,  $S$  is the riparian gradient towards the stream,  $n$  is Manning's coefficient, and  $t_o$  is interflow initiation time, which is computed as the time it takes for water to flow from the soil surface to the top of the impeding layer. The second part in

Equation 8 is related to the downslope travel time over the impeding layer, while the third component of the equation is a modification of Manning's equation for the duration of overland flow in the variable saturation area. The variable saturation distance requires knowledge of the stream reaches including the elevation and depth of groundwater in the riparian region, and how depth to groundwater responds to precipitation events; however, the latter is expected to be a minor factor relative to the downslope travel time because of the small variable saturation distance and faster surface flow as compared to flow in the subsurface. The simplifying assumption for  $V_d$  (variable saturation distance) involves the use of water body maps to identify stream cells and the wet riparian zones of the watershed, which are assumed to have a value of zero. Interflow initiation time ( $t_o$ ) varies based on the characteristics of the precipitation event (i.e., intensity, depth, pattern), the antecedent moisture condition, and the nature of the subsurface topography, especially in the active area. For a saturated condition of the topsoil layer with a thickness of 1.5 m, the time elapsed for the given effective rain to reach the surface of the impeding layer was estimated to be about 0.5 hr.

The total event-based interflow volume ( $V_{Tint}$ ), calculated according to Equation 7, was converted into a series of interflow rates ( $Q_i$ ) in  $m^3/hr$  using an empirical transformation function. A gamma-shaped transformation function of the form  $Q = t^\alpha e^{-t/\beta}$  was proposed to explain the shape of interflow hydrographs as recorded from the experimental hillslope. The time-variant transformation function generates an hourly travel distance distribution coefficient ( $C_i$ ) between  $t_i$  equal to zero and the interflow duration ( $t_{int}$ ) that was used as an input for routing  $V_{Tint}$ . The gamma function form given in Equation 10 showed suitable fits to the interflow hydrographs produced by the different distributions of event rain in the experimental hillslope. Equation 9 provides the flow rate ( $Q_i$ ) based on the calculated total interflow volume ( $V_{Tint}$ ), effective rain and amount leaking through the impeding layer over the interflow period (0 to  $t_{int}$ ).

$$V_{Tint} = \sum_{i=t_o}^{t_{int}} (Q_i) = \sum_{i=t_o}^{t_{int}} \left( \frac{C_i P_{eff} K_L \sin \alpha L}{\eta_d} \right) \quad (9)$$

$$C_i = k (t_i - t_o)^\lambda e^{-(t_i - t_o)/\beta} \quad (10)$$

where  $Q_i$  is the interflow at any time between 0 and  $t_{int}$ ,  $C_i$  is the travel distribution coefficient computed using Equation 10,  $\eta_d$  is the drainable porosity,  $L$  is the length of the stream receiving interflow, which needs to be multiplied by two when the stream receives flow from both stream banks,  $t_o$  is the interflow initiation time,  $t_i$  is the hourly time step between  $t = 0$  at start of event rain to  $t = t_{int}$ , and  $k$ ,  $\lambda$  and  $\beta$  are parameters that are fixed by the condition  $V_{Tint} = \sum Q_i$ .

In summary, the approach in the event-based model was carried out in three steps. Firstly, the total interflow volume ( $V_{Tint}$ ) and the possible interflow duration time ( $t_{int}$ ) were calculated based on event rainfall information, mainly the distribution of the event rainfall over time. Secondly, the shape transformation function was used to estimate the interflow rate at any given time by setting the free parameters in Equation 10 such that the condition in Equation 9 is satisfied.

The third step was to compute the interflow rate  $Q_i$  using the right side of Equation 9 ( $Q_i = C_i P_{eff} K_L \sin \alpha L / \eta_d$ ).

### 3 | MODEL APPLICATION AND FIELD MEASUREMENTS

#### 3.1 | Site description

The model was tested and validated using observations from an experimental hillslope within the USDA-Forest Service Upper Fourmile Creek experimental watershed at the Savannah River Site in South Carolina (Figure 3). The Upper Fourmile Creek experimental watershed is 11.1  $km^2$  and contains three smaller, intensively monitored headwater subwatersheds (R, B and C watersheds). These watersheds contain networks of soil moisture probes, groundwater and riparian water monitoring wells, an eddy covariance tower, five interflow collection trenches, stream flumes and rainfall gauges. Hydrologic observations in these watersheds began in 2008–2010. This analysis uses data from the experimental hillslope in the R watershed, primarily data from the interflow collection trench (Figure 3) (Du et al., 2016; Griffiths et al., 2016; Jackson et al., 2014, 2016; Klaus, McDonnell, Jackson, Du, & Griffiths, 2015). The interflow collection trench is a 121-m-long open trench that was cut into the impeding layer and along the contour of the experimental hillslope with a contributing area of 0.056  $km^2$  and a slope length of approximately 200 m to the ridgetop. In addition to the long-term observation record from the R experimental hillslope, a field-based irrigation experiment was also conducted there (described below and in Jackson et al., 2016).

The R experimental hillslope is gently sloping with typical slopes of 4–7%, up to 12%. Vegetation on the hillslope is mature loblolly pines and scattered hardwoods. Soils are Ultisols. The topsoils are well-drained loamy sands of the Fuquay soil series formed on marine terraces with a sand content of approximately 80–90%. The sandy A and E horizons overly an impeding argillic sandy clay loam Bt horizon with clay content of approximately 35%. The surface of the impeding layer is highly dimpled, and consequently, the depth to the impeding layer varies from 0.2 to 2 m (Du et al., 2016). The median hydraulic conductivities of the soils above the R trench, determined with a compact constant head permeameter, were 100 mm/hr for the topsoils and 5 mm/hr for the argillic horizon (Du et al., 2016). A steady-state irrigation experiment in the same area indicated average conductivities of 460 and 2.5 mm/hr for the topsoils and argillic horizon, respectively (Jackson et al., 2016). Dye tracers applied during the irrigation experiment indicated preferential flow path conductivities ranging from 864 to 2,240 mm/hr for the topsoils.

The climate is characterised by intense rain and an average annual rainfall of 1,250 mm that is distributed evenly throughout the year. The area is also characterised by hot summer and cold winter months. The historical climate observations show an average daily maximum temperature of  $\sim 33.5^\circ C$  between June to August and an average daily minimum temperature of  $1.5^\circ C$  between December and February



(Kilgo & Blake, 2005). Estimated annual potential ET is about 1,400 mm (Du et al., 2016).

### 3.2 | Data

The dynamic interflow modelling tool depends on the availability of detailed information on soil horizons in the hillslope. Soil parameters such as depth and Ksat values of the layers are used to determine a water budget for the soil profile and movement of water within and on the soil surface. Model calibration and validation require high-resolution hydroclimatic data, detailed soil parameters including the horizon (layer) hydraulic conductivities, porosity, average thickness of soil layers, depth of perching, water content at field capacity, wilting point, and saturation, and interflow and perching observations. At this time, the model does not account for variability in topsoil thickness. The types of data used in the analyses are described below.

Hourly potential ET rates were calculated using a modified Penman-Monteith method (Allen, Pereira, Raes, & Smith, 1998) based on climate observations at the Savannah River Site. We used combined 15-minute rainfall data from a tipping bucket rain gauge (located in the R watershed) and from a central meteorological tower located 1.5 km from the experimental hillslope. The central tower provided climatic data such as radiation, wind speed, temperature, relative humidity, pan evaporation and rainfall every 15 min. We aggregated the 15-minute climate datasets to hourly time steps from January 1, 2012 to December 31, 2013 for all of the analyses in this study.

Two unique interflow and perched water table datasets from the R experimental hillslope were used in the model analysis. The first is hourly interflow and perching depth triggered by rainfall from January 2012 to December 2013, and the second is an irrigation experiment

conducted upslope of the open trench in April 2012 during a period without rain. The trench is sub-divided into 11 segments each 11 m long and that collect and transport their respective lateral outflow to separate V-notch weir boxes (Figure 3). The trench observations represent perched water above the impeding layer and do not include surface runoff or deeper groundwater components. Once intercepted in the trench, the conveyance system is designed to prevent any transmission loss making it an ideal dataset for understanding the nature and magnitude of interflow. Beginning in 2010, Odyssey water-level probes, which have  $\pm 3$  mm accuracy according to the manufacturer's manual, were installed to measure water depth every 15 min in each weir box, and water depth was converted into a flow rate using a standard weir formula.

The irrigation experiment was conducted in April 2012 over a 198 m<sup>2</sup> area of the hillslope (green box in Figure 3) (see Jackson et al., 2016 for details on the irrigation experiment). The irrigation was applied on a 12 by 16.5 m area of hillslope using uniformly spaced sprinklers on 2 by 4 m grids. During this irrigation experiment, an equivalent to one-third of average annual precipitation was applied to initiate perching and interflow and achieve steady-state flow conditions through the impeding layer. The irrigation occurred in two consecutive stages. A high-intensity irrigation rate averaging 14 mm/hr was applied for the first 19 hr to saturate the soil and initiate perching quickly. Once a steady state was achieved, a lower irrigation rate up to 6 mm/hr was applied for 32 hr. Interflow was observed 12 hr after the irrigation began. A total of 407 mm of irrigation water was applied, and 201 mm left the system as interflow over 203 hr. The peak flow was observed after 55 hrs of irrigation. A nest of three piezometers were installed to measure the depth of the perched water table every 15 min using Odyssey water level probes: one at the impeding layer interface, one within the impeding layer and one below the impeding layer. This piezometer nest was located closer to the

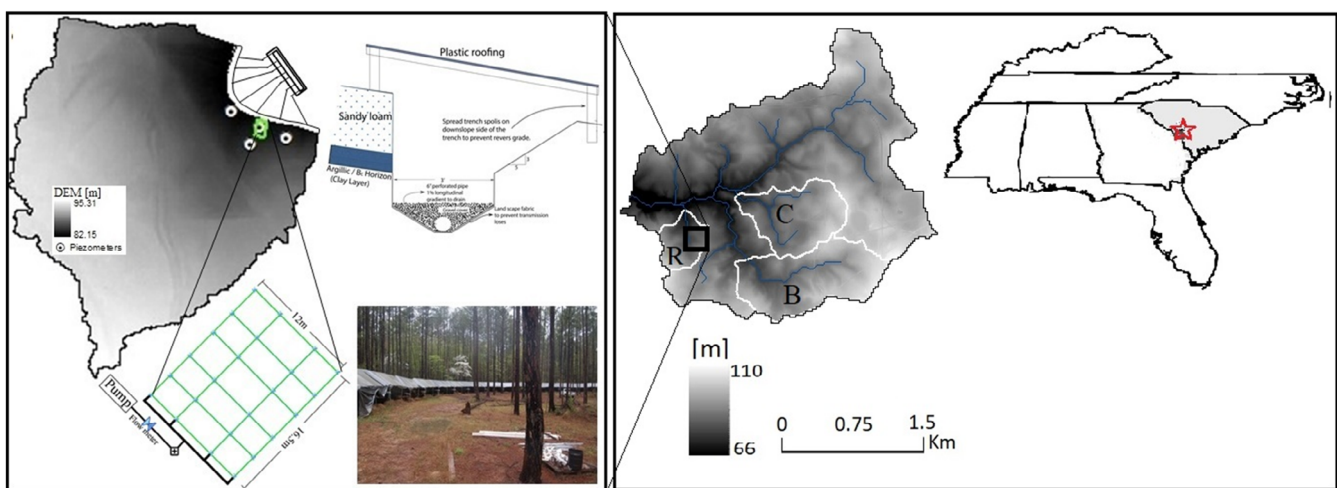


**FIGURE 3** Relief maps of the R experimental watershed used to model downslope travel distances. The downslope travel distance model was tested and developed using data from the 0.056 km<sup>2</sup> R experimental hillslope (left) in Upper Fourmile Creek watershed at the Savannah River Site in South Carolina, USA (right). The hillslope drains to a 121-m-long open interflow collector trench, which was fitted with 11 V-notch weir boxes and water-level measuring capacitance probes. An irrigation experiment took place on 198 m<sup>2</sup> of the hillslope (green grid) to understand and measure perching and interflow processes using a large, artificial rainfall event

edge of the trench and within the area of the irrigation experiment. While other piezometers were located on the hillslope, hourly data summarised from 15 min data from this nest of piezometers (Figure 3) were used in this modelling analysis because of some inconsistencies and data quality issues from other piezometers. One potential issue in using these piezometer measurements to estimate perching depth is related to the uncertainty in the location of the bottom of the piezometer with respect to the irregular surface of the impeding soil layer.

### 3.3 | Model calibration and performance evaluation

To mimic the flow processes, we calibrated the model parameters within ranges constrained by observations of the study site (e.g., Du et al., 2016; Jackson et al., 2016) and evaluated model predictions based on the observed datasets. Even though piezometer observations were part of the objective function, the performance evaluation was mainly focused on fitting the interflow hydrographs at hourly time steps. To use the limited piezometer and interflow observations, we conducted the calibration of the continuous model by separating the observations by year: 2012 and 2013. We applied a labour intensive manual calibration strategy (e.g., Bitew & Gebremichael, 2011; Boyle, Gupta, & Sorooshian, 2000) of the parameters in Table 1 to create a good fit between the observations and model predictions. Initially, we used visual inspection between the model predictions and the

continuous records (Bitew, Gebremichael, Gebremichael, & Bayissa, 2012; Van Liew, Arnold, & Bosch, 2005) and then applied statistical indicators such as the correlation coefficient (R), Bias and Nash Sutcliffe efficiency (NSE; Nash & Sutcliffe, 1970) to evaluate model performance. In the event-scale model, the soil properties remained the same as in the continuous model, but the parameters that described abstraction deficit and the ET components were made to vary.

## 4 | RESULTS

### 4.1 | Active area behaviour and extent

The model produces a dynamic interflow contributing area that expands and contracts from the bottom of the hillslope as a result of perching, downslope flow and leakage. The inclusion of leakage through the impeding layers limits the areal extent of near-surface lateral flow that contributes to stream flow. The size of the active area and the maximum downslope travel distance varies based on the effective precipitation depth (Figure 4). The parameters for computing the extent of the active area for a given rainfall were a conductivity value of 2,600 mm/hr and a depth of 1.5 m for the topsoil and a conductivity of 1 mm/hr for the underlying impeding layer. The conductivity values, which are at the upper end of the in situ measurements from the R-experimental hillslope, were the result of the calibration processes that produced the best interflow fits.

**TABLE 1** Dynamic downslope model parameters and calibrated values for Upper Fourmile watershed

Parameters	Unit	Notation	Value range	Measured	Calibrated values	
					Continuous model	Event-based model
Topsoil layer						
Hydraulic conductivity	m/hr	$K_u$		0.33–2.0	2.8	2.6
Saturation	$m^3/m^3$	$\Theta_s$	0.3–0.54		0.42	–
Field capacity	$m^3/m^3$	$\Theta_{fc}$	0.15–0.25		0.2	–
Wilting point	$m^3/m^3$	$\Theta_w$	0.01–0.1		0.01	–
Argillic layer						
Hydraulic conductivity	m/hr	$K_L$		0.002–0.003	0.001	0.001
Saturation	$m^3/m^3$	$\Theta_{as}$	0.3–0.35		0.35	–
Field capacity	$m^3/m^3$	$\Theta_{afc}$	0.1–0.2		0.25	–
Wilting point	$m^3/m^3$	$\Theta_{aw}$	0.01–0.05		0.1	–
Hillslope characteristics						
Depth of sand layer	m	$T$	1.5–2.0	1.3–1.5	1.5	1.5
Depth of clay layer	m	$d$	1.0–1.4	1.4–1.6	1.4	1.4
Porosity	–	$\eta$	0.25		0.41–0.35	0.35
Drainable porosity	–	$\eta_d$			0.3–0.1	0.1
Maximum canopy interception	Mm	$C_{max}$	3			
Canopy interception coefficient	–	$C_{in}$	0.02–0.05			
Detention storage	Mm	$i_c$	1–2	–	3.4	3.0
Gamma variables <sup>a</sup>	–	$\lambda, \beta,$ and $k$	–		–	

<sup>a</sup>Calibration parameters.



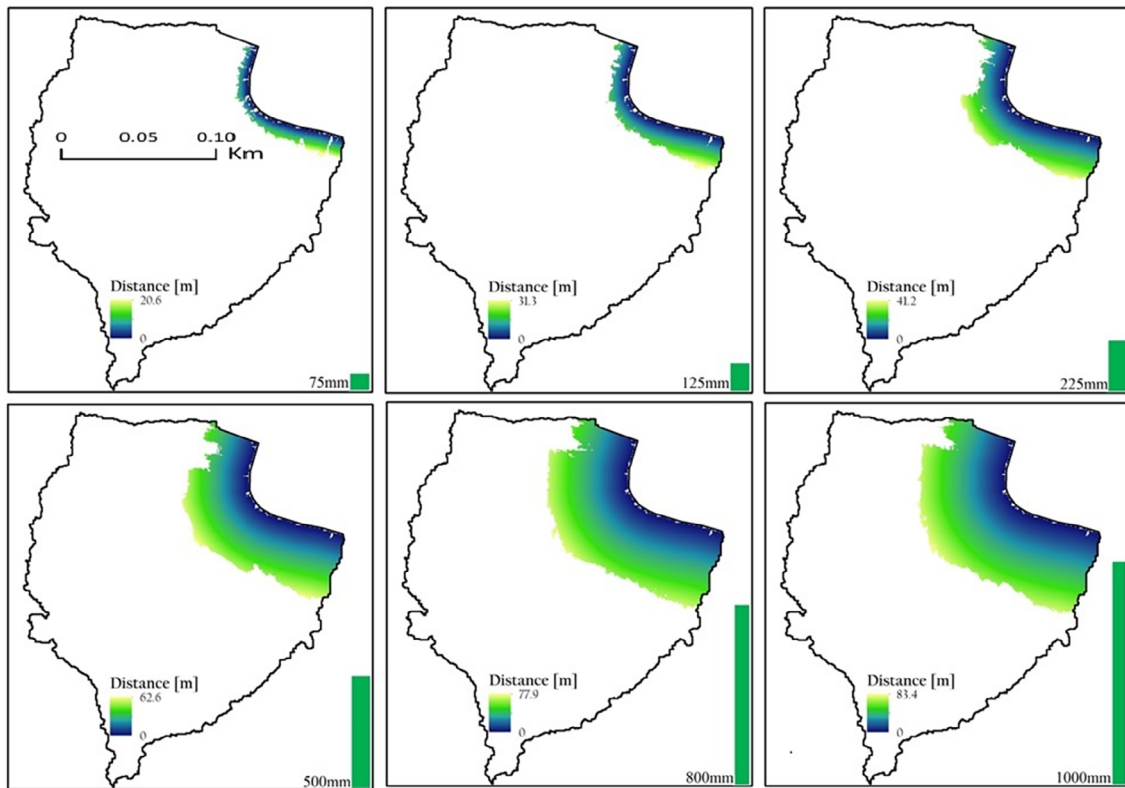


**FIGURE 4** Interflow contributing cells for a range of precipitation amounts that developed perching above the leaky impeding layer in the R experimental hillslope. Water parcels from colour-coded cells can flow down the slope and enter the stream as interflow. The different colours show downslope travel distance values of the active cells. The green bar (lower right in each panel) shows the depth of rain. The white portion of the watershed (upslope of the coloured region in each panel) represents inactive cells with respect to interflow, which indicates that any perched water in the white part of the watershed percolates to groundwater and does not reach the stream channel as Boussinesq (slope-parallel) flow

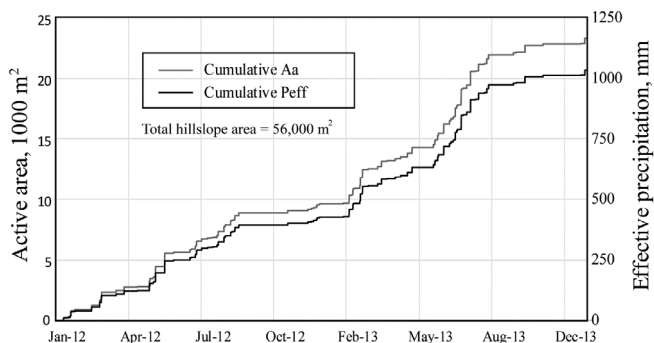


**FIGURE 5** Time series of the modelled cumulative active area ( $A_a$ ) in response to the effective precipitation ( $P_{eff}$ ). The active area developed with perched water storage above the impeding layer and subsided depending on the subsequent rainfall and amount of abstraction (leakage, evaporation and interflow)

The extent of the active area and the upslope contributing length in the R trench (Figure 4) increases with the depth of excess rainfall but never encompasses more than a third of the entire hillslope even with 1,000 mm of precipitation. The active area decreases after rainfall ceases as ET, percolation and outflow, which all depend on the slope and conductivity of the topsoil, continue to abstract water from the active portion of the hillslope. The model shows the active area of

interflow as the response to the effective precipitation that resulted in perching for the simulation period (Figure 5). An event-based analysis of the 2, 10 and 100 year return period for 24 hr of precipitation predicted contributing lengths of approximately 22, 28 and 34 m, respectively, compared to the total hillslope length of approximately 200 m (Figure 6). The fractions of hillslope area contributing to these events were 4.5, 6.8 and 8.6%, respectively. Even for a hypothetical storm of 1,000 mm (80% of annual precipitation), the active contributing length was 83 m and the active contributing area was 36.8% of the total hillslope area. Due to the convergent topography of the hillslope, the active contributing area did not scale linearly with storm size, and the marginal increase in contributing length and area diminished as storms got larger (Figure 6).

#### 4.2 | Continuous interflow prediction over a 2-year record

The continuous model predicted the presence of interflow/no interflow and perching/no perching with >90% accuracy regardless of interflow magnitude over 2 years of observation (2012–2013) (Figure 7). The Nash-Sutcliffe efficiency (NSE) value, %bias and a correlation coefficient (R) calculated at hourly time steps for data points

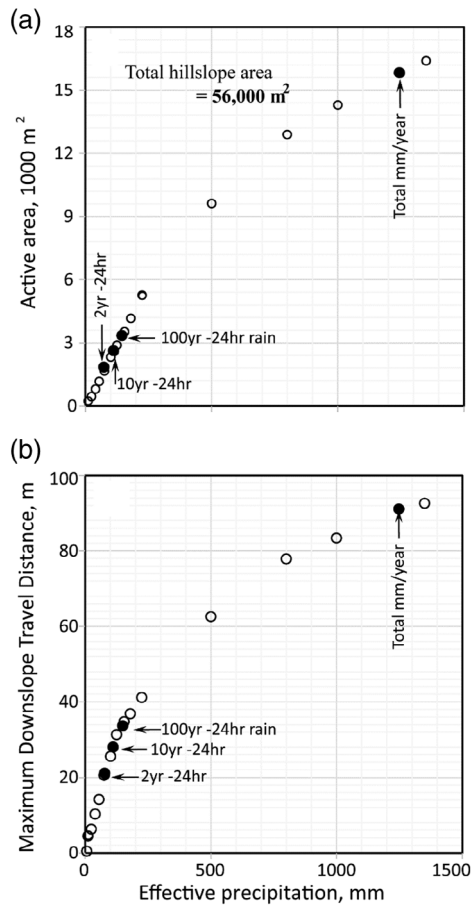


**FIGURE 6** Relationships between the (a) active area ( $A_a$ ) versus effective precipitation ( $P_{eff}$ ) and (b) maximum downslope travel distance ( $L_{Dmax}$ ) versus  $P_{eff}$  in the R experimental hillslope. The black circles show 2, 10 and 100-year events that last 24 hr, and total annual precipitation for the R watershed of 1,250 mm. The open circles represent the range of effective precipitation, from 0 to 1,300 mm

in 2013 were 0.5,  $-0.12$  and  $0.78$ , respectively (Figure 7a). The 2013 validation data showed a tendency to overestimate the predicted interflow, which is apparent in the comparison of observed and modelled cumulative interflow (Figure 8a). We also evaluated variability in model performance over two distinct validation periods: January 2013–July 2013 and July 2013–December 2013. The NSE and R of the first segment of the data (January 2013–July 2013) improved to  $0.52$  and  $0.81$ , respectively. The continuous model did not, however, accurately reproduce interflow depths due to a variety of simplifications of the flow environment, particularly the simplified representations of subsurface topography. A realistic representation of the rugged surface of the impeding layer instead of the simplified slope-parallel impeding layer would improve the performance of the model by capturing variability in the depth of the perched water table across the hillslope. The model performed poorly when predicting the magnitude of the perched water depth (Figure 7b) with the NSE  $<0$  and a correlation coefficient of  $0.35$  in the second segment of the data (July 2013–December 2013). The low predictability of perched water

depth (Figure 8b) with a coefficient of determination ( $R^2$ ) of  $0.26$  may also be related to single uniform values of conductivity and leakage rates assumed in the model. Past research at this site has shown that conductivities of the topsoil and the impeding layer are not uniform, and that both preferential downslope flow and leakage occur (Du et al., 2016; Jackson et al., 2016). None of these flow complexities can be practically included in model parameterization.

### 4.3 | Evaluation of perching and interflow time series predicted by the continuous and event-based models during individual perching events within the two-year simulation period

A total of 22 events generated interflow during the two-year study period. We used eight selected events for the event-based interflow analysis. The total interflow volume and the possible interflow duration were computed using the total event rainfall depth and related abstractions. Computed interflow volumes ( $V_{Tint}$ ) closely matched the observed interflow volumes (Figure 9a) with  $R^2$  values of  $0.85$  and  $0.84$  for the continuous and event models, respectively. The computed interflow duration ( $t_{int}$ ) estimates were respectable (Figure 9b) with  $R^2$  values of  $0.62$  and  $0.59$  for the continuous and event models, respectively. The general shapes of the simulated interflow hydrographs agreed fairly well with the interflow observations with no instabilities in the predicted water levels or flows (Figure 10), but the simulated interflow records were much smoother than the observations. The event-based approach reproduced observed interflow hydrographs better than the continuous model with NSE and correlation coefficients as high as  $0.93$  and  $0.98$ , respectively, for event-based prediction (Figure 10). Some of the events showed low predictive skill with small NSE values (e.g., Figures 10e,f,h), which could be related to limitation in the models, especially when the event rainfall consisted of multiple peaks that generated flat-topped interflow hydrographs. With such little interflow, measurement error in Odyssey water level probe recordings (i.e.,  $\pm 3$  mm accuracy) and the conversion to flow rate (in  $m^3/hr$ ) using the V-notch weir equation are all potential sources of uncertainty. The simulated peak flow rates (for both the continuous and event-based models) compared very well with observed peaks with  $R^2$  values better than  $0.85$  (Figure 9c). The shape transformation function parameters for the event-based model were selected by changing the values of  $k$ ,  $\lambda$  and  $\beta$  in Equation 10 in such a way to make  $\sum Q_i$  be equal to the computed  $V_{Tint}$ . The range of routing function parameter values (Figure 11) showed consistency in the type of hydrographs and distribution of rainfall causing interflow. In this exercise, we found  $\lambda$  and  $\beta$  parameters to be arbitrary while the  $k$  value seemed to depend on the distribution of rainfall. The  $k$  values of hydrographs with a quick rising limb and relatively slower receding limb (Figures 10a,b,h), which are usually caused by single storms, were set to relatively large values with an upper end of  $0.21$ . The hydrograph that showed steady flow, multiple peaks and a slow receding limb (e.g., Figures 10d,e,f, and Figure 12), which were

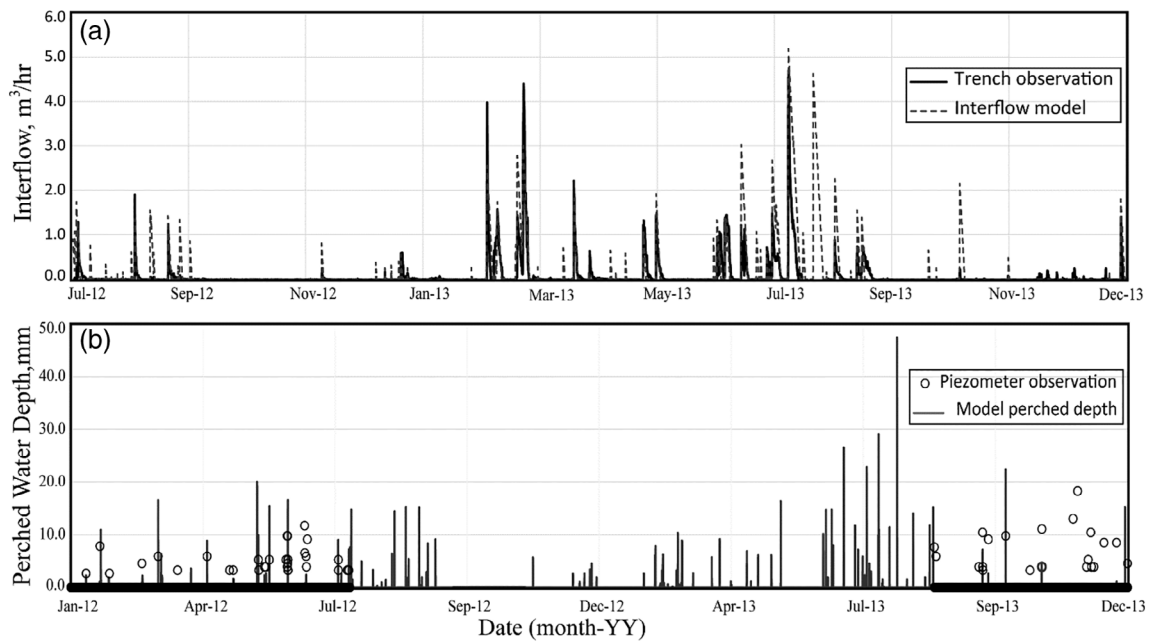


**FIGURE 7** Comparison of the dynamic downslope travel distance model estimates against observations of interflow and perched water table depth. (a) predicted interflow rate versus observed interflow in the 121-m open interflow collector trench at the R experimental hillslope, (b) predicted perched water table above the impeding layer vs. observed perching depth in nested piezometers in the R experimental hillslope. Note the x-axes of 'a' and 'b' are different

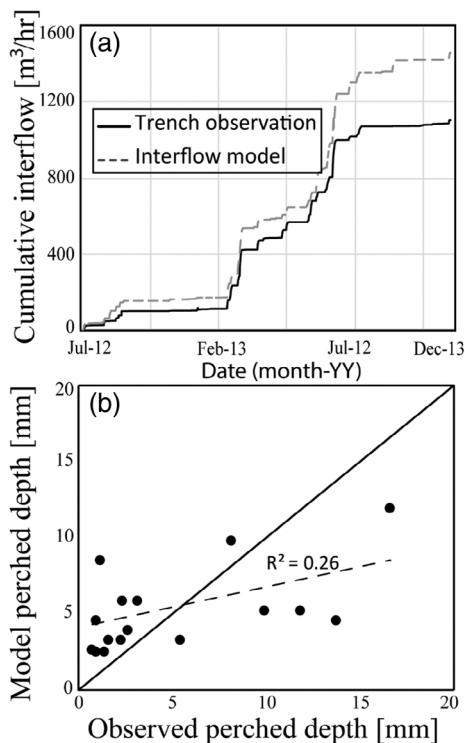


**FIGURE 8** Comparison of model predictions to observations of interflow and the depths of the perched water table from 2012 to 2013. (a) cumulative modelled and observed interflow and (b) observed versus modelled perched water depth, including a 1:1 line (solid line)

usually caused by successive storms, was set to a very small  $k$  as low as 0.000001. The interflow initiation time ( $t_o$ ) was set to a computed  $t_o$  value of 0.5 hr for all the hydrographs except for Figure 10b,c,h. For events in Figure 10b,c,h, interflow began about 21, 18, and 30 hr, respectively, after the beginning of the event rain. Hence,  $t_o$  values set to 21.5, 18.5 and 30.5 hr (Figure 11). The hourly interflow rates were calculated from 0 hr (i.e., the event rainfall starting time) to the total interflow duration ( $t_{int}$ ).

#### 4.4 | Application of the event-based model to the irrigation experiment

When applied to the irrigation-driven interflow event on the R experimental hillslope, the event-based model (Equation 7) predicted 199.5 mm interflow as a total interflow ( $V_{Tint}$ ) using soil land surface parameter values given in Table 1. The sum of the transformed rate ( $\sum Q_i$ ) using Equations 9 and 10 based on the same data in Table 1 resulted in a very similar interflow volume. The sum of the predicted interflow rate ( $Q_i$ ) closely matched the observed rate (Figure 12) and was within 1.2 mm or <0.5% of the observed flow with the predicted hydrograph tracking the shape of the observed flow rate well except for the peak. In this analysis, out of a total of 407 mm of rain applied to the hillslope over 51 irrigation application hours, 235 mm was computed as effective rainfall from which 199.5 mm was the predicted interflow. 172 mm of water was lost to evaporation and was used to fill the deficits in the soil during the experiment. The remaining

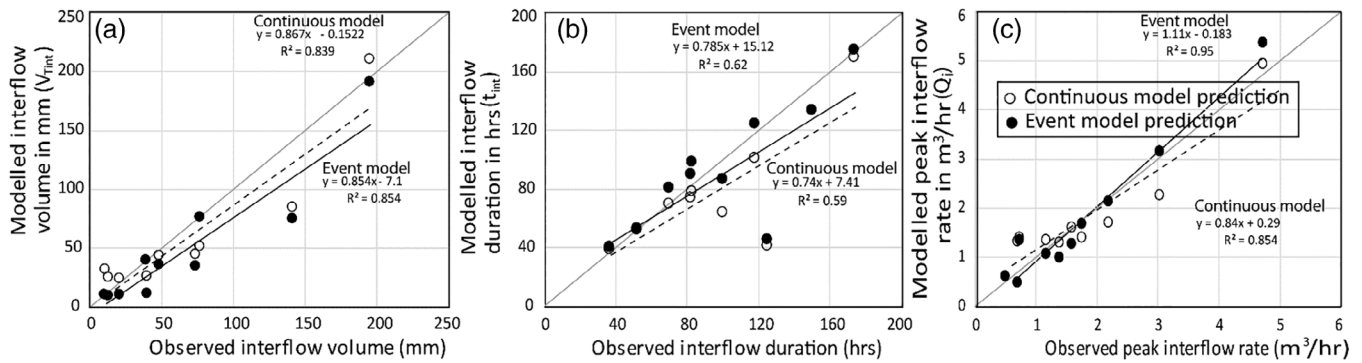


**FIGURE 9** Scatterplots of observed (x-axes) and modelled interflow (y-axes) parameters: (a) interflow volume, (b) interflow duration, and (c) peak interflow rate. The full circles represent results from the event-based model vs. observations, and the open circles represent results from the continuous model versus observations. The dashed trend line is for the continuous model and the solid line is for the event-based model

35 mm percolated below the impeding layer to the regional groundwater. The comparison of the flow rate (simulated vs. observed) showed an overestimation of the peak flow, which could be related to the uncertainty in the observed flow measurement, representation and assumptions of the uniform slope of the impeding layer, and model functions including the gamma transformation function used in the event-based model.

## 5 | DISCUSSION

Interflow can be an important component of hillslope runoff and should be included in hillslope and watershed models to better represent flow processes and hydrograph partitioning. Incorporating interflow dynamics is not only necessary to understand and quantify flow but also to describe the connectivity of the biologically active region of soil (topsoils) to the transport of solutes to streams (e.g., McGuire & McDonnell, 2010; Nippgen, McGlynn, & Emanuel, 2015). In many hydrologic models, the connectivity of perched water above a slope-parallel impeding layer is assumed to be continuous from the hilltop (e.g., Nippgen et al., 2015; Smith, Marshall, McGlynn, & Jencso, 2013; Troch et al., 2003, 2004). Several field studies have inferred continuous connectivity of perched water to streams (e.g., Jencso et al., 2009; Weiler & McDonnell, 2004; Zimmer & McGlynn, 2017). However, this is likely not the case in hillslopes with a leaky impeding layer (Klaus & Jackson, 2018). Including leakage in interflow models and evaluating the resulting changes in contributing areas fundamentally alter our views of hillslope transport.

This effort tested the idea that it is only necessary to model interflow production from the dynamic contributing area. The results indicate that this is a viable approach for estimating both interflow volumes and durations, as well as the extent of the active contributing area. The ability to predict the contributing area may be useful for the evaluation of solute transport including assessing the extent of mixing and potential impacts of the near-surface biogeochemically active riparian region on stream water quality. Understanding the processes and characterizing the features responsible for partitioning,

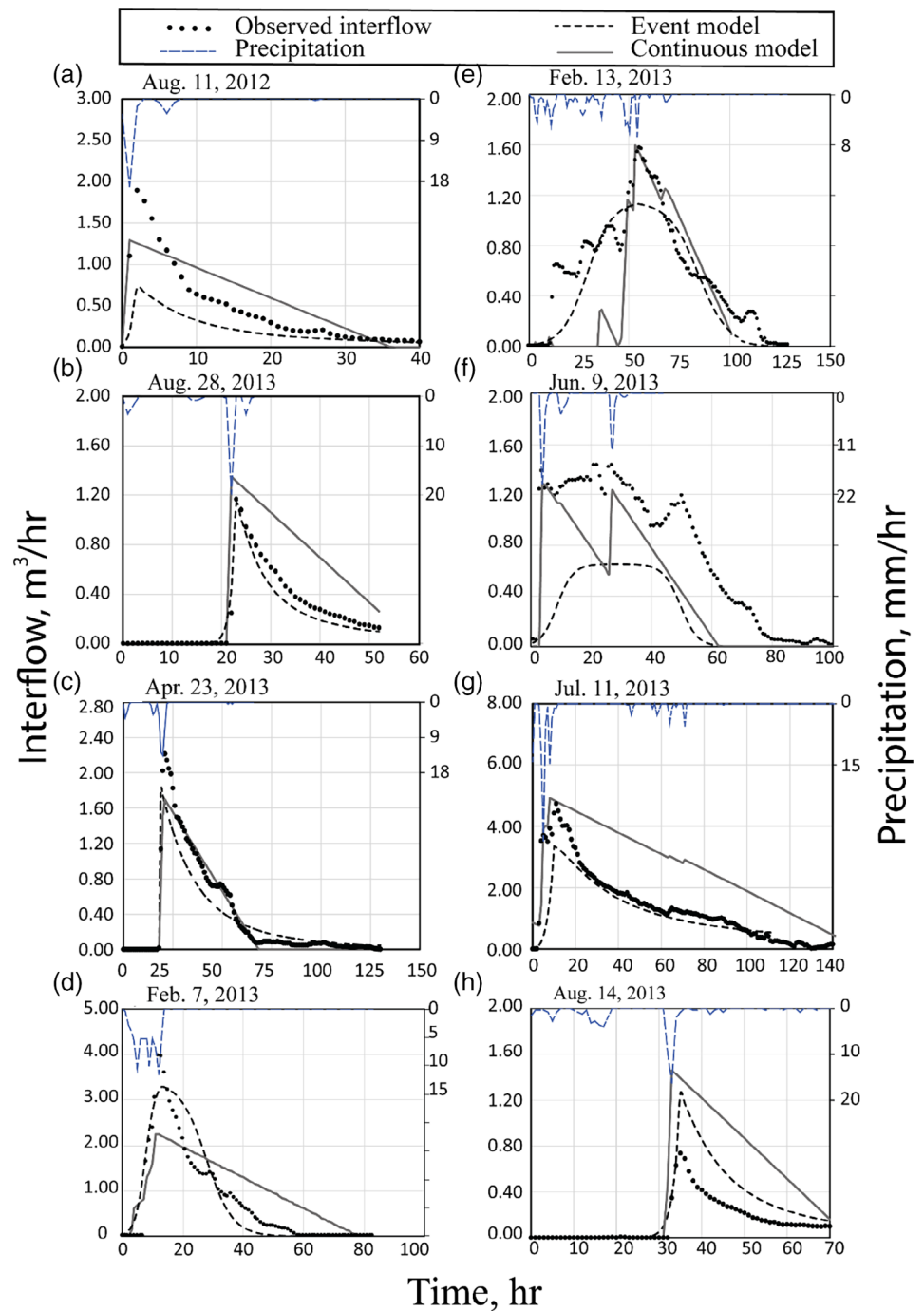
transporting and mixing waters in the biogeochemically active regions of the soil have paramount importance for catchment-scale water and land management.

These interflow models were not able to accurately predict perched water depths measured at individual piezometers on the hillslope. The impeding layer is modelled as parallel to the surface topography, but measurements in the R hillslope reveal that the argillic surface is dimpled, with low spots and high spots (Du et al., 2016; Jackson et al., 2016); these undulations are not included in the model. Similar variability in impeding layer topography has been observed elsewhere (Hale & McDonnell, 2016; Tromp-van Meerveld & McDonnell, 2006). In addition, some of the observational piezometers were placed in low spots in the argillic topography, and some in the high spots, and the uncertainty associated with the bottom position of the piezometers and top of the impeding layer may have also affected the poor prediction of perching depth. Including detailed subsurface topography in the model could improve the prediction of perching depths, but in most cases, there is minimal information on subsurface topography to bound the model domain.

## 6 | CONCLUSIONS

The downslope travel distance approach realistically represents interflow dynamics in hillslopes with leaky impeding layers and has the potential to be integrated with other process-based hydrologic modeling systems in order to more accurately represent catchment-scale hydrology. Using this concept, we created continuous and event-based interflow models that do not require an upslope boundary condition. The extent of leakiness of the impeding layer determines the downslope travel distance, and our findings suggest that perched water from the upper reaches of the hillslope will percolate through the impeding layer before reaching the valleys. Including leakage in a kinematic wave interflow model produced dynamic interflow contributing areas that expanded during storms and contracted afterwards as the perched water left the system through interflow, evapotranspiration and percolation to the groundwater.

**FIGURE 10** Comparison of modelled versus observed interflow hydrographs from the R experimental hillslope for selected events. Black dots represent observed interflow from the trench, the grey solid line is the estimated interflow from the continuous model, and the black dashed line is the estimated interflow from the event-based model. Precipitation is shown at the top of each panel as a blue dashed line. Statistics comparing the model fit to the field observations are provided on each panel



The continuous model predicted the occurrence, volume and peak of the interflow hydrographs, and the duration of perching very well and reasonably predicted the shape of interflow hydrographs at hourly time steps when compared to the observations. The continuous model did not, however, accurately reproduce interflow depths due to the simplified representations of subsurface topography. A realistic representation of the rugged surface of the impeding layer instead of the simplified slope-parallel impeding layer would improve the performance of the model by capturing variability in the depth of the perched water table across the hillslope.

The event-based model included assumptions and algorithms that produced rising limbs and recession curves of interflow hydrographs that better matched our field observations compared to the continuous model. The event-based model estimated the total volume of interflow and the time span over which interflow would be routed based on the physical distance water travels to the stream as interflow. Based on the limited observations from the R experimental hillslope, the gamma function type routing scheme seems to represent the shape of the hydrograph fairly well. However, this function requires further refinement to fit hydrographs with very long recessions, which can be caused by rain falling during the recession period



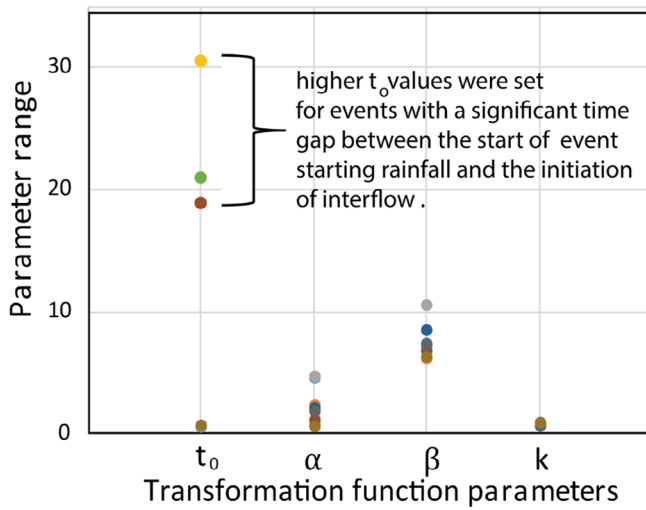


**FIGURE 11** The range in transformation function parameters determined for selected events using Equation 10 and the condition in Equation 9 to be satisfied. The colours represent the different events

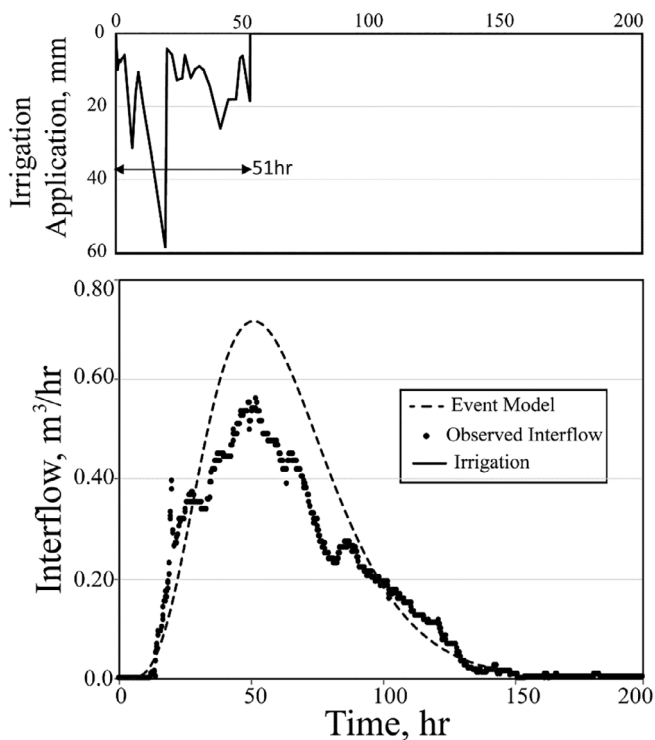


**FIGURE 12** Comparison of observed (dots) and predicted (dashed line) interflow at the R trench following the application of a total of 407 mm of water over 51 hr (top) as part of the irrigation experiment. Interflow was modelled using the event-based model

(e.g., Figure 10 g). In addition to the simplified representation of hillslope processes, it is also important to recognise the uncertainties in the sensor used to measure water level and uncertainties in calculating interflow from water-level data using the V-notch weir equation; these could impose additional layers of error on the observations,

especially for such small interflow outputs as those observed in the R hillslope. Long-term observations from different hillslopes are required to develop a universal transformation function to further improve the prediction of interflow hydrographs.

It is also important to mention that the integration of dynamic interflow modelling with other process-based hydrologic models may allow for more accurate partitioning of baseflow, interflow and runoff, leading to an overall better representation of the hydrograph properties of streams. In addition to understanding impacts of certain hillslope management interventions (e.g., effects of forest harvest), the dynamic interflow model can also help to describe hillslope connectivity, which is important for quantifying the transport of solutes above the impeding layer to adjacent streams and riparian regions. The demonstration of the application of the downslope travel distance concept in predicting interflow dynamics in hillslopes with leaky impeding layers and its potential for integration with other process-based hydrologic modelling systems will allow for future work to represent water quality and quantity processes more accurately at the catchment scale.

#### NOTATION

$K_u, K_L$	hydraulic conductivity of topsoil and impeding layer, respectively
$\Theta_s, \Theta_{as}$	soil moisture at saturation of topsoil and impeding layer, respectively
$\Theta_{fc}, \Theta_{afc}$	soil moisture at field capacity of topsoil and impeding layer, respectively
$\Theta_w, \Theta_{aw}$	soil moisture at wilting point of topsoil and impeding layer, respectively
$T$	depth of topsoil layer
$d$	depth of impeding layer
$\eta$	porosity of top layer
$\eta_d$	drainable porosity
$C_{max}$	maximum canopy interception
$C_{in}$	canopy interception coefficient
$i_c$	detention storage
$\lambda, \beta, k$	interflow hydrograph arbitrary parameters
$L_D$	downslope travel distance
$Nr_D$	nearest Euclidean distance down the hill to the stream
$Z_D$	hillslope elevation difference to the nearest stream
$\alpha$	hillslope angle
$C_n$	thickness of the impeding layer
$N$	normal depth of perched water on the hillslope
$V_d$	saturation variable distance in the riparian valley
$\Theta_i (\Theta_{ai})$	soil moisture content of topsoil and impeding layer, respectively
$P_d$	saturated soil depth above the impeding layer
$P_{eff}$	effective precipitation
AET	actual evapotranspiration
$A_a$	active area (area of interflow contributing hillslopes)
$t_o$	interflow initiation time
$V_{Tint}$	total interflow volume
$Q_i$	interflow rate over a given time step



$q_x, q_n$	lateral and vertical components of Darcy's velocity, respectively
$t$	average downslope travel time
$t_{\text{int}}$	interflow duration
$S, S_r$	Riparian zone average slope and hillslope, respectively.
$\sin(\alpha)$	
$n$	Manning's coefficient

## ACKNOWLEDGEMENTS

Funding and support were provided by the Department of Energy-Savannah River Operations Office through the U.S. Forest Service Savannah River under Interagency Agreement DE-AI09-00SR22188 and from the U.S. Department of Energy's Bioenergy Technologies Program to Oak Ridge National Laboratory. Oak Ridge National Laboratory is managed by UT-Battelle, LLC, for the U.S. Department of Energy under contract DE-AC05-00OR22725.

## CONFLICT OF INTEREST

The authors declared no conflict of interest.

## AUTHOR CONTRIBUTIONS

This manuscript has been co-authored by UT-Battelle, LLC under Contract No. DE-AC05-00OR22725 with the U.S. Department of Energy. The United States Government retains and the publisher, by accepting the article for publication, acknowledges that the United States Government retains a non-exclusive, paid-up, irrevocable, worldwide license to publish or reproduce the published form of this manuscript, or allow others to do so, for United States Government purposes. The Department of Energy will provide public access to these results of federally sponsored research in accordance with the DOE Public Access Plan (<http://energy.gov/downloads/doe-public-access-plan>).

## DATA AVAILABILITY STATEMENT

The data that support the findings of this study are available from the corresponding author upon reasonable request.

## ORCID

Menberu Meles Bitew  <https://orcid.org/0000-0002-1980-9243>

## REFERENCES

- Allen, R. G., Pereira, L. S., Raes, D., & Smith, M. (1998). *Crop evapotranspiration: Guidelines for computing crop water requirements* (Irrigation and Drainage Paper No. 56). Food and Agriculture Organization of the United Nations, Rome, Italy.
- Ambrose, B. (2004). Variable, 'active' versus 'contributing' areas or periods: A necessary distinction, invited commentary. *Hydrological Processes*, 18, 1149–1155.
- Asmussen, L. E., & Ritchie, J. C. (1969). Interflow or shallow phreatic flow in the coastal plain of Georgia. *Journal of Hydrology*, 9, 182–193.
- Beven, K. (1981). Kinematic subsurface stormflow. *Water Resources Research*, 17, 1419–1424.
- Bishop, K., Seibert, J., Kohler, S., & Laudon, H. (2004). Resolving the double paradox of rapidly mobilized old water with highly variable responses in runoff chemistry. *Hydrological Processes*, 18, 185–189.
- Bitew, M. M., & Gebremichael, M. (2011). Evaluation of satellite rainfall products through hydrologic simulation in a fully distributed hydrologic model. *Water Resources Research*, 47, W06526.
- Bitew, M. M., Gebremichael, M., Ghebremichael, L. T., & Bayissa, Y. A. (2012). Evaluation of high resolution satellite rainfall products through streamflow simulation in a hydrological modeling of a small mountainous watershed in Ethiopia. *Journal of Hydrometeorology*, 13(1), 338–350. <https://doi.org/10.1175/2011JHM1292.1>
- Boyle, D. P., Gupta, H. V., & Sorooshian, S. (2000). Toward improved calibration of hydrologic models: Combining the strengths of manual and automatic methods. *Water Resources Research*, 36, 3663–3674.
- Broda, S., Larocque, M., & Paniconi, C. (2014). Simulation of distributed base flow contributions to streamflow using a hillslope-based catchment model coupled to a regional-scale groundwater model. *Journal of Hydrologic Engineering*, 19, 907–917.
- Broda, S., Paniconi, C., & Larocque, M. (2011). Numerical investigation of leakage in sloping aquifers. *Journal of Hydrology*, 409, 49–61. <https://doi.org/10.1016/j.jhydrol.2011.07.035>
- Buttle, J. M., & McDonald, D. J. (2002). Coupled vertical and lateral preferential flow on a forested slope. *Water Resources Research*, 38, 1060.
- Clark, M. P., & Kavetski, D. (2010). Ancient numerical demons of conceptual hydrological modeling: 1. Fidelity and efficiency of time stepping schemes. *Water Resources Research*, 46, W010510.
- Du, E., Jackson, C. R., Klaus, J., McDonnell, J. J., Griffiths, N. A., Williamson, M. F., ... Bitew, M. (2016). Interflow dynamics on a low relief hillslope: Lots of fill, little spill. *Journal of Hydrology*, 534, 645–658.
- Dunne, T. (1978). Field studies of hillslope flow processes. In M. J. Kirkby (Ed.), *Hillslope hydrology* (pp. 227–293). Chichester: John Wiley & Sons.
- Flügel, W. A., & Smith, E. R. (1998). Integrated process studies and modeling simulations of hillslope hydrology and interflow dynamics using the HILLS model. *Environmental Modelling & Software*, 14, 153–160.
- Graham, C. B., & McDonnell, J. J. (2010). Hillslope threshold response to rainfall: (2) development and use of a macroscale model. *Journal of Hydrology*, 393, 77–93.
- Graham, C. B., van Verseveld, W., Barnard, H. R., & McDonnell, J. J. (2010). Estimating the deep seepage component of the hillslope and catchment water balance within a measurement uncertainty framework. *Hydrological Processes*, 24, 3631–3647.
- Griffiths, N. A., Jackson, C. R., McDonnell, J. J., Klaus, J., Du, E., & Bitew, M. (2016). Dual nitrate isotopes clarify the role of biological processing and hydrologic flow paths on nitrogen cycling in subtropical low-gradient watersheds. *Journal of Geophysical Research Biogeosciences*, 121, 422–437.
- Hale, V. C., & McDonnell, J. J. (2016). Effect of bedrock permeability on stream base flow mean transit time scaling relations: 1. A multiscale catchment intercomparison. *Water Resources Research*, 52, 1358–1374.
- Jackson, C. R., Bitew, M., & Du, E. (2014). When interflow also percolates: Downslope travel distances and hillslope process zones. Invited commentary. *Hydrological Processes*, 28, 3195–3200.
- Jackson, C. R., & Cundy, T. (1992). A model of transient, topographically driven, saturated subsurface hillslope flow. *Water Resources Research*, 28, 1417–1427.
- Jackson, C. R., Du, E., Klaus, J., Griffiths, N. A., Bitew, M., & McDonnell, J. J. (2016). Interactions among hydraulic conductivity distributions, subsurface topography, and transport thresholds revealed by a multi-tracer hillslope irrigation experiment. *Water Resources Research*, 52, 6186–6206.
- Jencso, K. G., McGlynn, B. L., Gooseff, M. N., Wondzell, S. M., Bencala, K. E., & Marshall, L. A. (2009). Hydrologic connectivity between landscapes and streams: Transferring reach-and plot-scale understanding to the catchment scale. *Water Resources Research*, 45, W04428.
- Kilgo, J. C., & Blake, J. I. (2005). *Ecology and management of a forested landscape*. Washington, D.C., USA: Island Press.

- Klaus, J., & Jackson, C. R. (2018). Interflow is not binary: A continuous shallow perched layer does not imply continuous connectivity. *Water Resources Research*, 54, 5921–5932.
- Klaus, J., McDonnell, J. J., Jackson, C. R., Du, E., & Griffiths, N. A. (2015). Where does streamwater come from in low relief forested watersheds? A dual isotope approach. *Hydrology and Earth Systems Science*, 19, 125–135.
- Koussis, A. D., Smith, M. E., Akylas, E., & Tombrou, M. (1998). Groundwater drainage flow in a soil layer resting on an inclined leaky bed. *Water Resources Research*, 34, 2879–2887.
- McGlynn, B. L., McDonnell, J. J., Shanley, J. B., & Kendall, C. (1999). Riparian zone flow path dynamics during snowmelt in a small headwater catchment. *Journal of Hydrology*, 222, 75–92.
- McGuire, K. J., & McDonnell, J. J. (2010). Hydrological connectivity of hillslopes and streams: Characteristic time scales and nonlinearities. *Water Resources Research*, 46, W10543.
- Minshall, N. E., & Jamison, V. C. (1965). Interflow in claypan soils. *Water Resources Research*, 1, 381–390.
- Nash, J. E., & Sutcliffe, J. V. (1970). River flow forecasting through conceptual models part I - A discussion of principles. *Journal of Hydrology*, 10(3), 282–290. [https://doi.org/10.1016/0022-1694\(70\)90255-6](https://doi.org/10.1016/0022-1694(70)90255-6)
- Newman, B. D., Campbell, A. R., & Wilcox, B. P. (1998). Lateral subsurface flow pathways in a semiarid ponderosa pine hillslope. *Water Resources Research*, 34, 3485–3496.
- Nippgen, F., McGlynn, B. L., & Emanuel, R. E. (2015). The spatial and temporal evolution of contributing areas. *Water Resources Research*, 51, 4550–4573.
- Pi, Z., & Hjelmfeld, A. T., Jr. (1994). Hybrid finite analytic solution of lateral subsurface flow. *Water Resources Research*, 30, 1471–1478.
- Schroeder, P. R., Gibson, A. C., & Smolen, M. D. (1983). *The hydrologic evaluation of landfill performance (HELP) model* (Vol. 2, pp. 25–28). Springfield, VA: National Technical Information Services Documentation of version 1, EPA/DF-85/OO1B, new.
- Sloan, P. G., & Moore, I. D. (1984). Modeling subsurface stormflow on steeply sloping forested watersheds. *Water Resources Research*, 20, 1815–1822.
- Sloan, P. G., Morre, I. D., Coltharp, G. B., & Eigel, J. D. (1983). *Modeling surface and subsurface stormflow on steeply sloping forested watersheds*. Water Resources Institute Report 142. Lexington, KY, University of Kentucky.
- Smith, R. E., & Hebbert, R. H. B. (1983). Mathematical simulation of interdependent surface and subsurface hydrologic processes. *Water Resources Research*, 19, 987–1001.
- Smith, T., Marshall, L., McGlynn, B., & Jencso, K. (2013). Using field data to inform and evaluate a new model of catchment hydrologic connectivity. *Water Resources Research*, 49, 6834–6846.
- Troch, P. A., Paniconi, C., & van Loon, E. E. (2003). Hillslope-storage Boussinesq model for subsurface flow and variable source areas along complex hillslopes: 1. Formulation and characteristic response. *Water Resources Research*, 39, 1316.
- Troch, P. A., van Loon, A. H., & Hilberts, A. G. (2004). Analytical solution of the linearized hillslope-storage Boussinesq equation for exponential hillslope width functions. *Water Resources Research*, 40, W08601.
- Tromp-van Meerveld, H. J., & McDonnell, J. J. (2006). Threshold relations in subsurface stormflow: 2. The fill and spill hypothesis. *Water Resources Research*, 42, W02411.
- Tromp-van Meerveld, H. J., Peters, N. E., & McDonnell, J. J. (2007). Effect of bedrock permeability on subsurface stormflow and the water balance of a trenched hillslope at the Panola Mountain research watershed, Georgia, USA. *Hydrological Processes*, 21, 750–769.
- van Genuchten, M.T. (1980). A Closed-form Equation for Predicting the Hydraulic Conductivity of Unsaturated Soils 1. *Soil Sci. Soc. Am. J.*, 44, 892–898.
- Van Liew, M. W., Arnold, J. G., & Bosch, D. D. (2005). Problems and potential of autocalibrating a hydrological model. *Transactions of the ASAE*, 48(3), 1025–1040.
- Weiler, M., & McDonnell, J. (2004). Virtual experiments: A new approach for improving process conceptualization in hillslope hydrology. *Journal of Hydrology*, 285, 3–18.
- Wilcox, B. P., Newman, B. D., Brandes, D., Davenport, D. W., & Reid, K. (1997). Runoff from a semiarid ponderosa pine hillslope in New Mexico. *Water Resources Research*, 33, 2301–2314.
- Zaslavsky, D., & Sinai, G. (1981). Surface hydrology: IV flow in sloping, layered soil. *Journal of the Hydraulics Division*, 107(1), 53–64.
- Zimmer, M. A., & McGlynn, B. L. (2017). Ephemeral and intermittent runoff generation processes in a low relief, highly weathered catchment. *Water Resources Research*, 53, 7055–7077.

**How to cite this article:** Meles Bitew M, Jackson CR, Goodrich DC, et al. Dynamic domain kinematic modelling for predicting interflow over leaky impeding layers. *Hydrological Processes*. 2020;1–16. <https://doi.org/10.1002/hyp.13778>